# MRR
# Physical Basics

Version 5.2.0.1

METEK
Meteorologische Messtechnik GmbH

Last update :  11 July 2009

# Table of Contents

# 1 MRR Characteristics

## 1.1 Short Description

The MRR Micro Rain Radar is a compact 24 GHz FM-CW-radar for the measurement of profiles of drop size distributions and – derived from this – rain rates, liquid water content and characteristic falling velocity resolved into $30^1$ range gates. Due to the high sensitivity and fine temporal resolution very small amounts of precipitation – below the threshold of conventional rain gauges – are detectable. Due to the large scattering volume (compared to in situ sensors) statistically stable drop size distributions can be derived within few seconds. The droplet number concentration in each drop-diameter bin is derived from the backscatter intensity in each corresponding frequency bin. In this procedure the relation between terminal falling velocity and drop size is exploited.

## 1.2 Radar Frequency

The backscatter cross section of rain drops increases with the fourth power of the radar frequency, if the target diameter is small compared to the wavelength (Rayleigh scattering). This is why a high frequency is useful in order to increase the sensitivity with respect to small drops.
At very high frequencies the quantitatively interpretable height range becomes limited due to attenuation at moderate and higher rain rates. At 24 GHz, which is used here, attenuation effects may be noticeable but should be weak enough to be correctable with sufficient accuracy.

## 1.3 Radar-Frontend

The core component of the radar is a frequency modulated gunn-diode-oscillator with integrated mixing diode. The nominal transmit power is 50 mW.
The assembly and function of the radar frontend is explained with reference to the block diagram in figure 1. The linear polarized rf-power is fed through a wave guide and a horn, which represents the feed of an offset paraboloid dish of 60 cm diameter (not shown).
The backscattered signal is received with the same antenna assembly (monostatic radar). The received signal is detected by a mixing diode which is mounted in the wave guide between gunn-oscillator and horn. This diode, which is biased with a fraction of the transmit signal, acts as mixer. This simple configuration cannot be operated in pulsed mode, because during the shut off of the transmitter, the receiver does not work either. When operated in continuous wave mode, a voltage appears at the diode output, which depends on the phase difference between the transmit and receiving signal (homodyne principle), and which is used for the further signal processing.

---

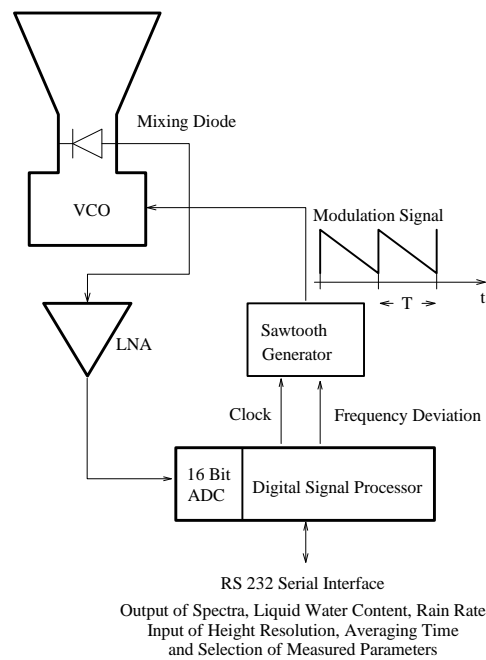[1] MRR-2 only (MRR-1: 6 range gates)

Figure 1: Block diagram MRR

## 1.4 FM-CW-Method

### 1.4.1 Resting Point Target

As the radar module cannot be operated in pulsed mode, the range of a target cannot be derived in the usual way, i.e. from the time elapsed between transmission of a pulse and reception of an echo. In order to achieve range resolution the transmit signal is frequency modulated, and the range of the target (or the time lag of the received echo) is derived from the frequency shift between the echo and the transmit signal. Here a linearly decreasing frequency modulation (saw tooth) of the transmit signal is used. In the upper part of figure 2 the frequency of the transmit signal and the frequency of the echo from a resting point target is shown. Due to the time delay of the echo its frequency is always higher than that of the transmit signal, and the frequency difference is proportional to the range of the target. The frequency sweeps linearly from $f_0 + B/2$ to $f_0 - B/2$ and jumps back to the initial value. The frequency jump of the echo follows somewhat later with the delay $t_h = 2\ h/c$, with $h$ range of the target and $c$ velocity of light. The time interval $t_h$ between the frequency jumps of the transmit and the receiving signal is not used for the further signal processing. This interrupt is small compared to $T$, the time of a full frequency sweep. In the lower part of figure 2 the corresponding output of the mixing diode is shown. Its frequency is equal to the constant frequency difference $f$ between the transmit- and the receiving-signal.
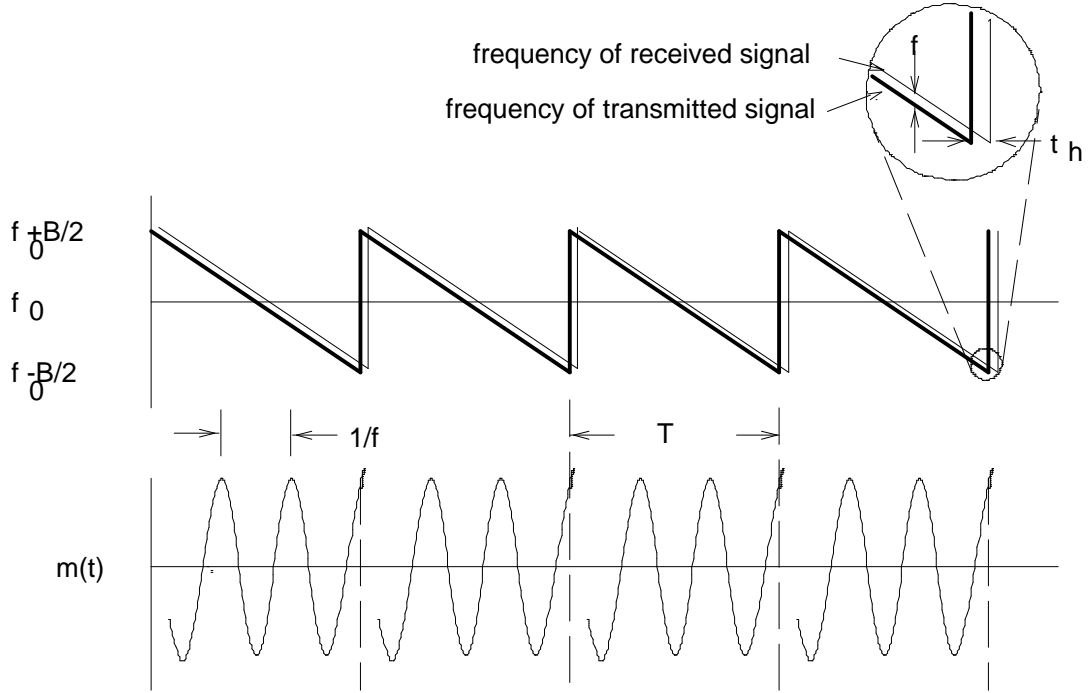
Figure 2: Resting point target
Upper part: Frequency of the transmit signal and the echo. Lower part: Mixer output

### 1.4.2  Range Resolution

The transmit signal be described by the function

$$s(t) = S \sin(\varphi_S(t))$$                                          (1.4.2.1)

where the phase $\varphi_s(t)$ is the integral of the "instantaneous" cycle frequency $\int \omega_S(t)dt$. During one sweep holds the relation

$$\omega_S(t) = \omega_0 - 2\pi \frac{B}{T} t \quad \text{for} -T/2 \leq t \leq T/2$$          (1.4.2.2)

Thus the transmit signal reads

$$s(t) = S \sin\left(\omega_0 t - 2\pi \frac{B}{2T} t^2\right)$$                    (1.4.2.3)

The receiving signal is delayed with respect to the transmit signal by $t_h = 2h/c$, i.e. its phase is $\varphi_e(t) = \varphi_s(t - t_h)$ or

$$e(t) = E \sin\left(\omega_0 t - \omega_0 t_h - 2\pi \frac{B}{2T}\left(t^2 - 2t_h t + t_h^2\right)\right)$$          (1.4.2.4)

"Mixing" means basically multiplying  of *s(t)* and *e(t)*. If both signals are described by sinusoidal functions, the product can be written as sum of two sinusoidal functions, where the phase of the first term is equal to the sum of the phases of *s(t)* and *e(t)* and the phase of the second term is equal to the difference of the phases of *s(t)* and *e(t)*. We assume that the frequency deviation *B* is small compared to the center frequency $f_0$. Then the first term is very high frequent as compared to the second term. The frequency of the first term is about 2 $f_0$. Its contribution to the mixing signal is suppressed by a low pass filter, and only the second term is considered further. The phase of the second term is

$$\varphi_m(t) = \overbrace{\omega_0 t - \omega_0 t_h - 2\pi \frac{1}{2}\frac{B}{T}t^2 + 2\pi \frac{B}{T}t_h t - 2\pi \frac{1}{2}\frac{B}{T}t_h^2}^{\varphi_e(t)} \overbrace{- \omega_0 t + 2\pi \frac{1}{2}\frac{B}{T}t^2}^{-\varphi_S(t)} \qquad (1.4.2.5)$$

The frequency of the mixing signal is derived by differentiation of its phase with respect to time: $f_m = (1/2\pi)\ \partial\varphi_m(t)/\ \partial t$. Applying this to equation (1.4.2.5) yields

$$f_m = B\frac{t_h}{T} \qquad (1.4.2.6)$$

Two targets can be resolved only, if they are separated by a distance corresponding to a frequency difference of at least one line, which is $\delta f = 1/T$, if one sweep of duration *T*  is analyzed. From equation (1.4.2.6) follows that there is the relation

$$\delta t_h = \frac{T}{B}\delta f \qquad (1.4.2.7)$$

between the time-delay resolution $\delta t_h$ and the frequency resolution $\delta f$. Replacing $\delta f$ by *1/T* in equation (1.4.2.7)  and considering, that $\delta t_h$ and the spatial resolution $\delta h$ are related by $\delta h = (1/2)\ c\ \delta t_h$, yields

$$\delta h = \frac{1}{2}\frac{c}{B} \qquad (1.4.2.8)$$

In summary, the relation between bandwidth and range resolution does not differ essentially from that which holds also for a conventional pulse radar, considering the relation between band- and pulsewidth.

### 1.4.3  Moving Point Target

The echo of a moving target exhibits an additional frequency shift, which is proportional to the velocity according to the Doppler effect.
Thus there appears an ambiguity between range and velocity. In fact this ambiguity could not be resolved, if the echo would be analyzed only during one single sweep. Then the frequency resolution of the FFT would be *1/T*, and there would be no FFT-lines between adjacent harmonics. The frequency shift observed during one sweep is

$$\Delta f_{total} = \underbrace{\frac{2}{\lambda}v}_{Doppler} + \underbrace{B\frac{2h}{cT}}_{range} \qquad (1.4.3.1)$$

We now consider the echo of a "slowly" moving point target for a series of sweeps as shown in figure 3. The beat signal of each sweep is Fourier (1st FT) transformed. The complex spectral lines, presented in polar co-ordinates are indicated by arrows. Each spectral line represents one range gate $r$. In figure 3 the lower 10 range gates are shown ($0 \leq r \leq 9$). The MRR analyses 32 range gates. Here the point target is located in the middle between range gate 3 and 4, so that the spectral power is equally distributed in line 3 and 4. In this example the target is approaching the radar at a speed of

$$v = \lambda / 8T \tag{1.4.3.2}$$

i.e. the position of the target is moved by $\lambda / 8$ from one to the next sweep. As this is small compared to the depth of the range gate, the position of the target is still between range gate 3 and 4, but the phase of the echo is advanced by 90° between subsequent sweeps. We now interpret the complex spectral voltage in each range gate as a new time series, which is sampled at the rate $1/T$. The Fourier tansformation of each of these time series yields power spectra with a line resolution of $1/nT$. The unambiguous frequency range (Nyquist-range) of the 2nd FT comprises the interval $f_N = 1/T$. In our example maxima of spectral power appear in the power spectra of range gate 3 and 4 at the frequency

$$f_D = f_N / 4 \tag{1.4.3.3}$$

Comparison of equations (1.4.3.2) and (1.4.3.3) show that $f_D = 2v / \lambda$, which is just the relation for the Doppler velocity. We conlude that the spectra resulting from the 2nd FT can be interpreted as Doppler spectra of the corresponding range gate.

The separation of range and velocity is only possible if the uncertainty of the target velocity is within the Nyquist interval. In case of falling rain drops we assume a positive frequency shift. So the frequency is unambiguous in the interval $0 \leq f_D < f_N = 1/T$. The width of the Nyquist interval can be controled by chosing the sweep repetition rate $1/T$.
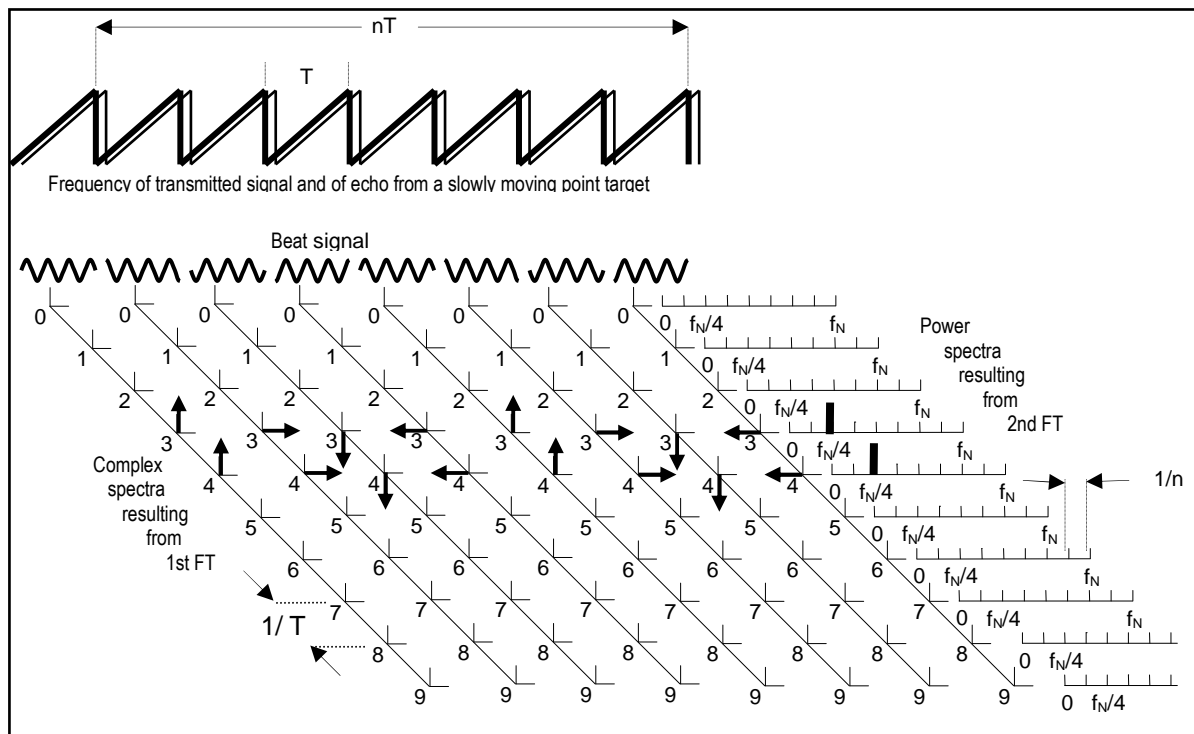
Figure 3: Slowly moving point target
Echo in the time and frequency domain

### 1.4.4  Scattering at Raindrops

In case of rain always a large number of drops exists within the scattering volume. A typical number density at moderate rain (1 mm/h) is 2000 m$^{-3}$. The scattering volume (500 m height, 50 m range resolution) has a size of about $10^4$ m³, i.e. $2 \cdot 10^7$ drops are in the scattering volume. As the drop position is irregular in space the phases of the scattering signals of each drop are statistically independent. Therefore, the total power of the echo is obtained by adding up the power of all individual scattering signals.

In this case the spectrum within one range gate consists of a distribution of lines corresponding to the velocity distribution of the rain drops. The frequency spectra obtained in this way with the FM-CW radar do not differ within the Nyquist interval from those spectra which would be obtained by a pulsed Doppler radar with the same wave length.

## 1.5  Spectral processing

### 1.5.1  Incoherent Averaging

The spectral power of a single power spectrum obtained from a high number of targets, randomly distributed within the scatterin volume, contains a large stochastic component due to the arbitrary phases of all superposed signal contributions. Incidently, the standard deviation of the power is just equal to the expectation value of the power. It is therefore desirable to reduce the stochastic component by averaging ensembles of power spectra. Averaging over $n$ power spectra reduces the standard deviation by $1/\sqrt{n}$  in the limit of
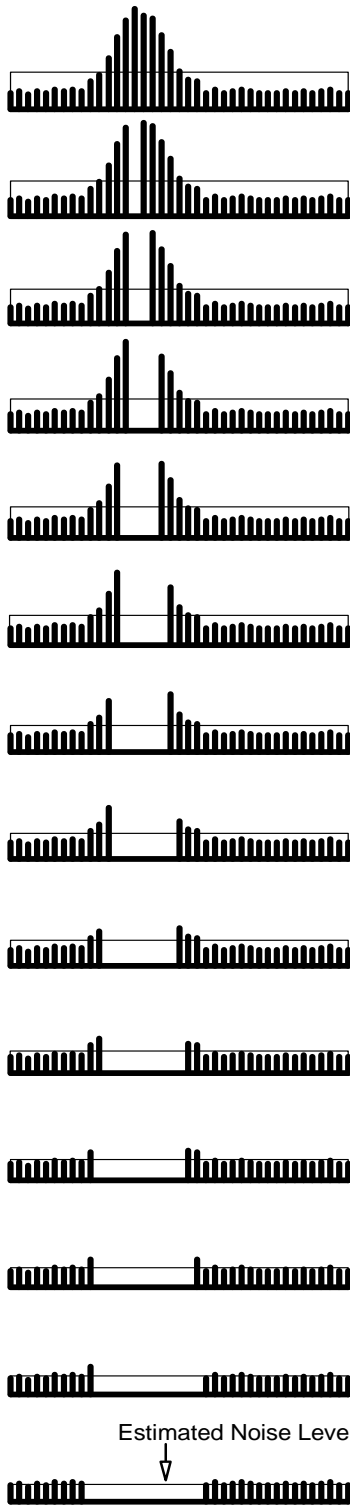
Estimated Noise Level

Figure 4: Estimation procedure of the noise level. The thin horizontal lines indicate the mean spectral power, of the remaining spectral lines.

$n \gg 1$. The DSP of the MRR generates about 25 power spectra per second, which is about 80% of the real time value. In the standard setting of operating parameters the DSP transfers averaged spectra every 10 s to the data acquisition unit. The data transfer time takes about 4 s. During this time no measurement is possible. This means that the net averaging interval is 6 s in this case, which contains 150 single power spectra. Thus the stochastic standard deviation of spectral powers is reduced to 8% or 0.34 dB.

### 1.5.2  Noise Estimation

In addition to the echo signal some unavoidable noise is present at the input of the radar receiver. If this would be ignored, an apparent rain rate would be detected. Even this false rain rate is small, its persistence could result in a significant bias of the accumulated rain fall. (Real rain occurs only in few percent of the total measuring time, depending on the climate zone and season.)

Therefore a noise estimation module is included in the signal processing procedure. For this purpose some feature of noise must be assumed, which allows the discrimination of noise from signal. Here it is assumed that the noise is "white" (frequency independent) in the analyzed Doppler range. Similar as for the signal, the spectral noise powers show a stochastic variability which is equal to that of the signal namely 8 % or 0.34 dB for the above mentioned settings of operation parameters. The noise level is estimated as indicated in fig. 4: In the first step the mean power of the spectrum is calculated. Then the spectral line with the maximum power is removed, and the spectral power is calculated again. If it is equal or larger than the previous estimate, the procedure stops and the calculated mean power is identified with the noise power. If it is smaller (as in this example), the procedure is continued. The spectral line with maximum power located left or right to the previously removed spectral line is removed and so on. In this example the procedure stops after removal of the 12th spectral line. The estimated spectral noise power is subtracted from each spectral line before further processing of the spectra.

# 2  Derivation of Drop Size Distributions

The raw spectral power $f(n,i)$ received by the radar (recorded in engineering units) is

$$f(n,i) = \frac{10^{20} \cdot \text{TF}(i)}{C} \frac{1}{i^2 \Delta h} \eta(n,i) \qquad (2.1)$$

$n$ is the line number of the Doppler spectrum ( $n = 0...63$ ),
$i$ is the number of the range gate ( $i = 1....32$ ),
TF($i$) and $C$ are the transfer function and calibration constant as given in the header of the output data,
$\Delta h$ is the range resolution in units ms$^{-1}$,
$\eta(n,i)$ is the spectral reflectivity, i.e. the backscatter cross section per volume in units m$^{-1}$.

The PC-resident program **MRR2-control**, which is described in **MRR Control User Manual, Version 4.2**, uses TF($i$) and $C$ stored in the MRR-firmware.

The "instantaneous" and "average" reflectivity spectra provided by the on-line processing are corrected for the noise floor and for attenuation. The are displayed in logarithmic scale "dBη":

$$F(n,i) = 10 \cdot \log \eta(n,i) \qquad (2.2)$$

The Doppler velocity of line $n$ is

$$v(n) = n \cdot \Delta v = n\Delta f \cdot \lambda / 2 \qquad (2.3)$$

with $\Delta f = 30.52\,\text{Hz}$ frequency resolution of the Doppler spectra corresponding to the velocity resolution $\Delta v = \Delta f \cdot \lambda / 2 = 0.1905\,\text{ms}^{-1}$ .

For the derivation of drop size distributions the relation between terminal fall velocity $v$ and drop diameter $D$ is used, which has been found empirically by Gunn and Kintzer (1949), and which has been put into an analytical form by Atlas (1973), (see Figure 5). We use a generalized form, in which a height dependent density correction for the fall velocity $\delta v(h)$ is included.

$$v(D)[\text{m/s}] = \left(9.65 - 10.3 \cdot \exp(-0.6 \cdot D[\text{mm}])\right)\delta v(h) \quad \text{for } 0.109 \leq D \leq 6 \text{ mm} \qquad (2.5)$$

We assume US Standard Atmosphere conditions for the height dependence of air density, and we make use of the relation of Foote and duToit (1969), who found $v \propto \rho^{0.4}$. A second order approximation for $\delta v(h)$ under these assumptions is:

$$\delta v(h) = \left[ 1 + 3.68 \cdot 10^{-5} h + 1.71 \cdot 10^{-9} h^2 \right] \tag{2.6}$$


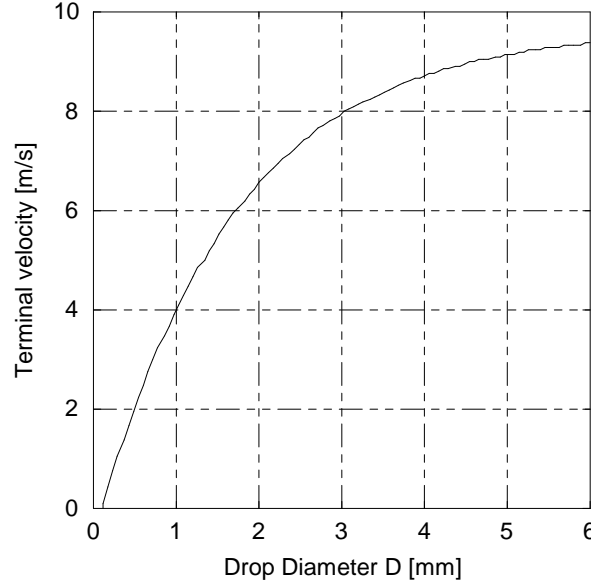
Figure 5: Terminal fall velocity of rain drops at the surface $(h = o)$ versus drop size in motionless air.

We introduce the spectral reflectivity density with respect to velocity $\eta(v,i) = \eta(n,i) / \Delta v$ and can derive from that the spectral reflectivity density with respect to the drop diameter.

$$\eta(D,i) = \eta(v,i) \frac{\partial v}{\partial D} \tag{2.7}$$

Inserting $\partial v / \partial D \left[ ms^{-1} mm^{-1} \right] = 6.18 \cdot \exp(-0.6 \cdot D \,[mm]) \delta v(h)$   (according to equation (2.5)) yields

$$\eta(D,i)[m^{-1}\, mm^{-1}] = \eta(v,i) \cdot 6.18 \cdot \mathbf{exp}(-0.6\, mm^{-1} \cdot D[mm]) \delta v(i \cdot \Delta h) \tag{2.8}$$

Dividing $\eta(D,i)$ by the single particle backscattering cross section $\sigma(D)$ of a rain drop of diameter $D$ yields the drop size distribution $N(D,i)$, i.e. number of drops per volume and diameter:

$$N(D,i) = \frac{\eta(D,i)}{\sigma(D)} \tag{2.9}$$

Equation (2.9) together with equation (2.8) represents a relation between the Doppler spectra and the drop size distributions, if the backscattering cross section $\sigma(D)$ is known.

For drop diameters small compared to the wavelength it could be expressed analytically (Rayleigh approximation):

$$\sigma_R(D) = \frac{\pi^5}{\lambda^4} \left| \underbrace{\frac{m^2-1}{m^2+1}}_{K} \right|^2 D^6,$$
(2.10)

where $m$ is the complex refractive index of water. $|K|^2$ of water at 24 GHz is about 0.92. (For ice spheres $|K|^2 = 0.18$). As the MRR wavelength is not small compared to all naturally occurring drop diameters the Rayleigh approximation is not applicable here. Instead of this $\sigma(D)$ is calculated according to Mie theory. In figure 6 the single particle scattering cross section, relative to the Rayleigh approximation is shown as it is used in the MRR drop size retrieval. The diameter is defined here and in the following as the volume equivalent sphere diameter: $D = \left(6V/\pi\right)^{1/3}$ with $V =$ volume of the drop.
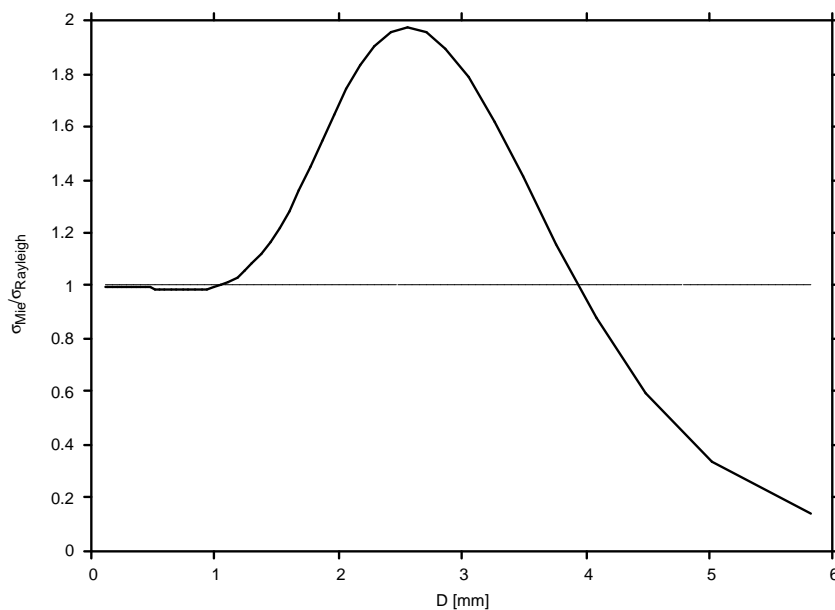


Figure 6: Single particle backscatter cross section of water droplets at 24.1 GHz normalized with Rayleigh backscatter cross section

The **MRR2-control** program calculates the rain drop size distributions for each range gate. The distributions are resolved in discrete steps which are equidistant in the Doppler velocity domain. The step width is $\Delta v$. The corresponding output parameter is N$nn$ as described in the **MRR Control User Manual, Version 5.2.0.1**.

Although 64 velocity steps from $nn = 0$ to 63 corresponding to $v = 0$ to 12.285 m/s are calculated primarily, equation (2.8) is applied only in the size range $0.246\,\text{mm} \le D \le 5.03\,\text{mm}$ corresponding to the height-normalized velocity range $0.78\;\text{m/s} \le v/\delta v(h) \le 9.34\,\text{m/s}$. Due to the height dependent fall velocity of a given drop size, the limits of the analyzed velocity range is height dependent as well. The retrieval

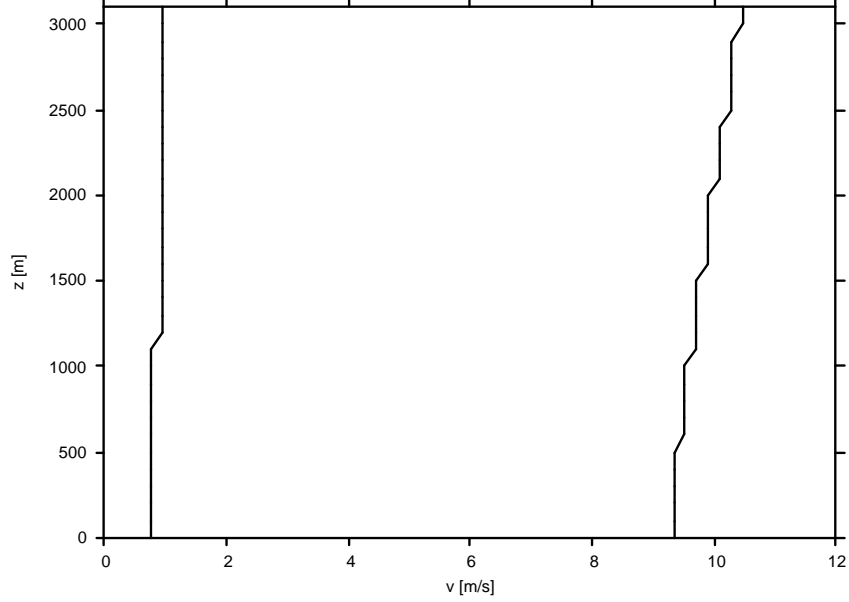interval is adjusted in full line increments, which introduces a steplike-structure as indicated in figure 7.



Figure 7: Retrieval range of velocity as function of height

# 3  Derivation of Rain Parameters

## 3.1  Spectral summation versus integration

By appropriately weighted integration of the spectral reflectivity density, various integral rain parameters as for example liquid water content or rain flux can be obtained.

In case of the **MRR** all integrations are replaced by summations over lines $nn$ from line $\min(h)$ to line $\max(h)$. At the surface $(h = 0)$ is $\min(0) = 4$ and $\max(0) = 49$. The variation of min and max with height is indicated in figure 7.

$$\int_0^\infty g(f)df \rightarrow \sum_{\min(h)}^{\max(h)} g_{nn} \tag{3.1.1}$$

where $g(f)$ represents a spectral density and

$$g_{nn} = g(f_{nn})\Delta f_D \tag{3.1.2}$$

the corresponding spectral power within the line $nn$ of width $\Delta f_D = 30.52$ Hz

Spectral densities with respect to $v$ are obtained by

$$g(v) = g_{nn} \frac{\partial f}{\partial v} \frac{1}{\Delta f} \tag{3.1.3}$$

$$\text{with } \frac{\partial f}{\partial v} \frac{1}{\Delta f} = \frac{1}{0.1905 \left[\text{ms}^{-1}\right]} \tag{3.1.4}$$

and spectral densities with respect to $D$ are obtained by

$$g(D) = g_{nn} \frac{\partial f}{\partial v} \frac{1}{\Delta f} \frac{\partial v}{\partial D} \tag{3.1.5}$$

$$\text{with } \frac{\partial f}{\partial v} \frac{1}{\Delta f} \frac{\partial v}{\partial D} \left[\text{mm}^{-1}\right] = 3.15 \cdot \left(9.65 \cdot \delta v(h) - v \left[\text{ms}^{-1}\right]\right) \tag{3.1.6}$$

If we insert in equation (3.1.5) for $g_{nn}$ the spectral reflectivity $\eta(n,i)$, as defined in equation (2.2), we obtain the spectral reflectivity density $\eta(D)$, which can be used immediately to calculate the drop size distribution $N(D)$ according equation (2.9).

## 3.2  Drop size distribution with attenuation correction

The intensity of radar waves is attenuated on the propagation path by different processes. Although the absorption by water vapour is relatively strong at 24 GHz (0.2 dB/km for $\rho_{water\ vapour} = 10$ g/m³), it is neglected on the path lengths considered here. But rain can attenuate significantly at moderate and higher rain rates, if high altitudes are considered. This would lead to a height dependent underestimation of rain rates

In the following we mark the variables without attenuation correction by the index $_a$ (not attenuation corrected) in order to distinguish between attentuation corrected and uncorrected variables. The specific rain attenuation is denoted by $\kappa$, the path integrated rain attenuation is denoted by $\textbf{PIA}$, the range resolution is denoted by $\Delta r$, the range number is indicated by $i$, and the single particle extinction coefficient is denoted by $\sigma_e$. It is calculated with Mie theory. The calculation starts in the first range gate $i = 1$. We assume that $\textbf{PIA}(r_0) = 1$.

1. Calculate $N_p(D_{nn}, r_i) = N_a(D_{nn}, r_i)\textbf{PIA}(r_{i-1})$

2. Calculate $\kappa_p(r_i) = \sum\limits_{\min(h)}^{\max(h)} \sigma_e(D_{nn})N_p(D_{nn}, r_i)dD$

3. Calculate $N(D_{nn}, r_i) = -N_p(D_{nn}, r_i)\textbf{ln}(1 - 2\kappa_p(r_i)\Delta r)/(2\kappa_p(r_i)\Delta r)$

4. Calculate $\kappa(r_i) = \sum\limits_{nn\_\min(h)}^{nn\_\max(h)} \sigma_e(D_{nn})N(D_{nn}, r_i)$

5. Calculate $\textbf{PIA}(r_i) = \textbf{PIA}(r_{i-1})\textbf{exp}(2\kappa(r_i)\Delta r)$

6. If $\textbf{PIA}(r_i) > 10$, exit.

7. Set $i = i + 1$, Go to 1.

A detailed justification of this algorithm has been submitted for publication and can be provided on request.

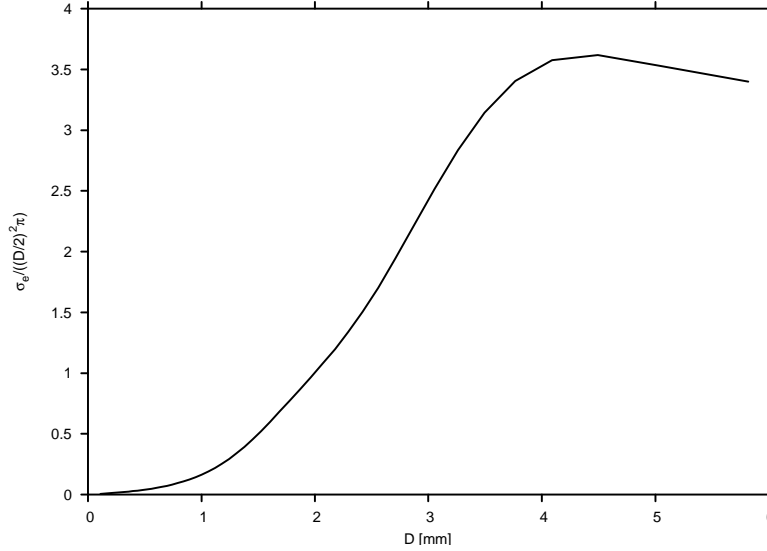

Figure 8: Single particle extinction coefficient of rain drops at vertical incidence normalized with the geometric crossection versus volume equivalent sphere diameter.

The attenuation correction is only applied for **PIA** $\leq 10$ because the algorithm becomes unstable for large values. Although no quantitaive rain retrieval is possible for larger attenuations the echoes do often contain still useful information, as for example the fall velocity which is not affected by attenuation. Therefore some of the retrieved variables are provided both with and without attenuation correction. The uncorrected values are dislayed also for **PIA** $> 10$. See MRR Manual for further details.

## 3.3 Equivalent Radar Reflectivity Factor

The radar reflectivity factor is defined by

$$Z = \int_0^\infty N(D)D^6 dD \tag{3.3.1}$$

For large wavelength (like for X-band radars) the Rayleigh approximation for small drops compared to the wavelength is valid, so that usually the equivalent radar reflectivity factor is used:

$$Z_e = \frac{\lambda^4}{\pi^5}\frac{1}{|K|^2}\int_0^\infty \eta(f)df \tag{3.3.2}$$

In our case Equation (3.3.2) is not aplicable due to the small wavelength of the MRR so that the Rayleigh approximation is no longer valid. For comparison with long wave weather radars $Z$ is calculated on the basis of the drop size distribution issued by the MRR using equation (3.3.1).

## 3.4  Liquid Water Content

The liquid water content is the product of the total volume of all droplets with the density of water $\rho_w$, divided by the scattering volume. It is therefore proportional to the 3rd moment of the drop size distribution:

$$LWC = \rho_w \frac{\pi}{6} \int_0^\infty N(D)D^3 dD \qquad (3.4.1)$$

## 3.5  Rain Rate

The differential rain rate *rr(D)* is equal to the volume of the differential droplet number density *(π/6) · N(D)D³* multiplied with the terminal falling velocity *v(D)*. From this product the rain rate is obtained by integration over the drop size:

$$RR = \frac{\pi}{6} \int_0^\infty N(D)D^3 v(D)dD \qquad (3.5.1)$$

## 3.6  Characteristic Falling Velocity

Various definitions for the characteristic falling velocity are possible. A physical reasonable definition would be the velocity of those drops which deliver the maximum contribution to the total rain rate. Another – here chosen – possibility is to determine the first moment of the Doppler spectra, because this is the usual way of radar wind profilers to determine radial velocities.

$$W = \frac{\lambda}{2} \int_0^\infty \eta(f)f df \left/ \int_0^\infty \eta(f)df \right. \qquad (3.6.1)$$

It is also possible to derive – on the basis of the drop size distribution – the first moment of those Doppler spectra which are expected in case of Rayleigh scattering. This would be an even better emulation of velocities observed by long-wave radar wind profilers. For this purpose one can use the issued drop size distribution to calculate the spectral "Rayleigh" reflectivity $\eta_R(D) = N(D)\sigma_R(D)$ and insert for the backscattering cross section $\sigma_R$ of equation (2.10).
This leads to the spectral Rayleigh reflectivity as function of *f*:

$$\eta_R(f) = \frac{N(D)\sigma_R(D)}{(\partial f / \partial v)(\partial v)(\partial D)} \qquad (3.6.2)$$

The characteristic "Rayleigh-velocity" is obtained by inserting $\eta_R$ into equation (3.6.1).

# 4 Error Considerations

## 4.1 Statistical Error of the Spectral Reflectivity

As with any volume targets with random internal structure the resulting spectral power is randomly distributed due to the uncorrelated phases of the individual contributing scattering targets. As a general rule the standard deviation of the spectral power distribution in each frequency bin is equal to its mean value.
Due to the limited data rate of the serial interface of the MRR the minimum measuring cycle time has been set to 10 s. Issuing the spectra via the interface takes about 4 s. During this time no measurement is possible due to spurious interferences from the active data port to the low noise receiving amplifier. Thus 6 s net measuring time are available with this setting of cycle time. 23 spectra per second are calculated and averaged incoherently, i.e. an issued spectrum represents a mean of a minimum of 138 single spectra. In this way the above mentioned statistical fluctuations are reduced to about 9 % of there mean values. For longer averaging times this variation is reduced proportional to the square root of the net-measuring time. Thus this error should be usually negligible – particularly for the integral parameters.

## 4.2 Vertical Wind

For the relation terminal falling velocity versus drop size (equation (2.5)) stagnant air had been assumed. In real atmosphere the drops are carried with the wind. Thus the velocity of equation (2.5) is relative to the ambient air velocity. Downwind, for example, increases the falling velocity, and application of equation (2.5) leads to an overestimation of the drop size. As the scattering cross section depends with high power on the drop diameter, equation (2.8) leads in this case to an underestimation of the number concentration. Thus, also the liquid water content and the rain rate is underestimated in the case of down wind. Quantitative estimates of this error and also of the errors discussed in the following sections can be found in Richter (1993) – in the limit of Rayleigh scattering and under the assumption of Marshal-Palmer drop size distributions. Based on simultaneous in-situ measurements of the vertical wind at 100 m height for a period of several months, the actual error associated with the assumption of zero vertical wind is demonstrated in figure 9. Each measurements represents 1 min average. No significant mean bias is recognized. While it is self evident that the mean vertical wind is zero over a plain surface the same cannot by taken for granted for its effect on the uncorrected rain rate, because this effect is not linear. A further potential reason for mean effects of the vertical wind is, that rain shafts may be correlated with vertical wind. Obviously also this correlation has only marginal consequences in the long term mean. The standard deviation of $10\log(R_{corr}/R_{uncorr})$ is about 1 dB. No dependence of the standard deviation on rain rates is observed. In one of about 10,000 observations the uncorrected estimate is low by 12 dB.
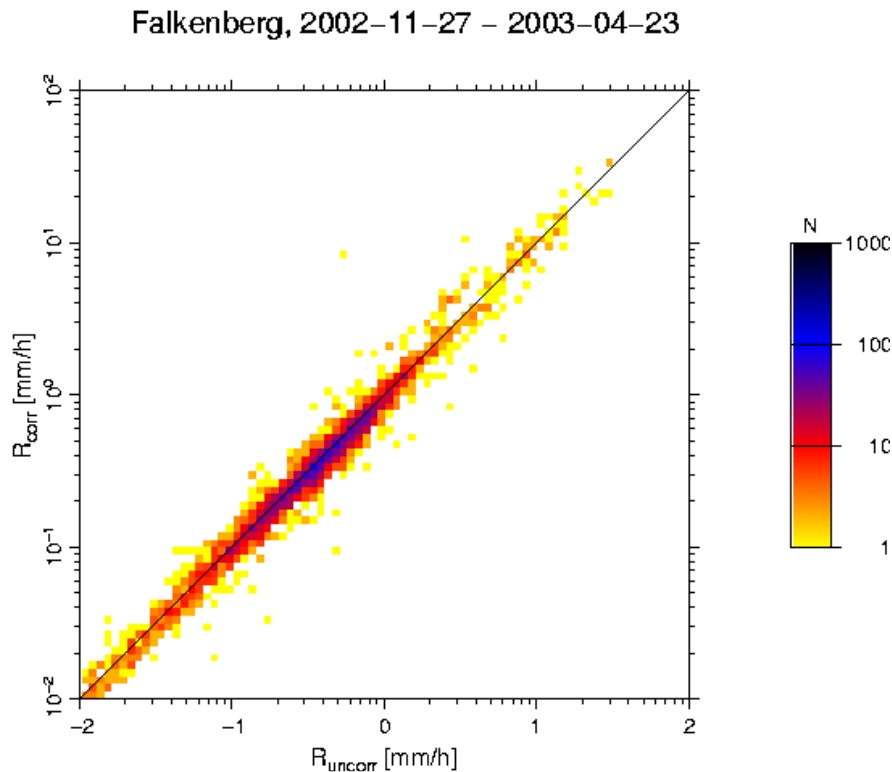
Figure 9: Comparison of rain rates with and without vertical wind correction.

## 4.3  Radar Calibration

The derived volume reflectivity, drop size distribution and all integral parameters depend proportional on the radar calibration constant *C*. It is determined by comparison with in situ rain rate measurements in selected environmental conditions. Its uncertainty is estimated to be ±10 %. The temporal stability of *C* has been investigated by evaluating the echo from a well defined target (triple reflector) and by changing the transmitter/receiver temperature over a range of about 30 K. The observed variation of echo power was less than 10 %. (These measurement cannot be performed with the standard signal processing software because echoes from fixed targets are suppressed.)

## 4.4  Ice Phase

The complex refractive index of ice is very different from that of water in this frequency range. The effect of this difference on the radar reflectivity is partly compensated by the difference of shape between water drops and ice crystal aggregates. Particularly in the melting layer (height with 0 °C) the radar reflectivity is even increased in comparison to the underlying altitudes with rain. The built-in signal analysis of the MRR always assumes the presence of liquid rain drops. Due to the smaller falling velocity of snow flakes in comparison to rain drops the rain rate and liquid water content is drastically overestimated in snow. Thus the melting layer can be very clearly recognized as an apparent maximum of rain rate (more clearly than by the backscattered power).

# References

Atlas, D., R. Srivastava und R. Sekhon, 1973: Doppler radar characteristics of precipitation at vertical incidence, Rev. Geophys. Space Phys., 11:1-35.

Foote, G. B., and duToit, P.S., 1969: Terminal velocity of raindrops aloft, J. Appl. Meteorol., 8:249-253.

Gunn, R. und G. Kintzer, 1949: The terminal velocity of fall for water droplets in stagnant air, J. Meteor., 6:243-248.

Klugmann, D. und C. Richter, 1995: Correction of Drop Shape-Induced Errors on Rain Rates Derived from Radar-measured Doppler Spectra at Vertical Incidence, J. Atmos. Ocean. Tech., 12, 657-661.

Richter, C., 1993: Niederschlagsmessungen mit dem vertikal gerichteten FM-CW-Dopplerradar-RASS-System, Validierung und Anwendung, Dissertation Universität Hamburg, 143 pp.

Strauch, R.G., W.C. Campbell, R.B. Chadwick, K.P. Moran: FM-CW boundary layer radar with Doppler capability, NOAA Techn. Rep. ERL 329-WPL 39, Dept. of Commerce, May 1975.